



Article

Outdoor Radon and Its Progeny in Relation to the Particulate Matter during Different Polluted Weather in Beijing

Cong Yu , Yuan Sun and Nanping Wang * 

School of Geophysics and Information Technology, China University of Geosciences (Beijing), 29 Xueyuan Road, Beijing 100083, China; congyu@email.cugb.edu.cn (C.Y.); 2010140041@email.cugb.edu.cn (Y.S.)

* Correspondence: npwang@cugb.edu.cn

Abstract: This study aimed to investigate the differences in the relationship between radon and its progeny concentrations and particulate matter concentrations under varying pollution weather conditions. Outdoor radon and its progeny concentrations were measured by a radon/thoron- and radon/thoron progeny monitor (ERS-RDM-2S) during haze and dust storm weather in Beijing. Particulate matter concentrations and meteorological data were simultaneously recorded. Results showed that radon and its progeny concentrations exhibited a diurnal variation pattern, with a minimum in the late afternoon and a maximum in the early morning. The average radon concentrations were similar under both pollution weather conditions, but significantly higher than the reported average for Beijing. The equilibrium equivalent radon concentration during haze was about two times that during a dust storm. PM10 concentrations were similar in both pollution weather conditions, but PM2.5 concentrations during haze were approximately 2.6 times higher than that during dust storms. A positive correlation was observed between radon and its progeny concentrations and particulate matter concentrations, but the correlation was significantly higher during haze than during dust storms. The higher PM2.5 concentration during haze significantly increased the correlation between radon and its progeny concentrations and particulate matter concentrations. We recommended protecting against radon exposure during pollutant weather, especially haze.

Keywords: radon and its progeny; particulate matter; haze; dust storm



Citation: Yu, C.; Sun, Y.; Wang, N. Outdoor Radon and Its Progeny in Relation to the Particulate Matter during Different Polluted Weather in Beijing. *Atmosphere* **2023**, *14*, 1132. <https://doi.org/10.3390/atmos14071132>

Academic Editors: Qiuju Guo and Miroslaw Janik

Received: 12 June 2023

Revised: 2 July 2023

Accepted: 7 July 2023

Published: 9 July 2023



Copyright: © 2023 by the authors. Licensee MDPI, Basel, Switzerland. This article is an open access article distributed under the terms and conditions of the Creative Commons Attribution (CC BY) license (<https://creativecommons.org/licenses/by/4.0/>).

1. Introduction

Radon and its progeny are classified as one of the major human carcinogens and are the second most common cause of lung cancer after smoking [1,2]. The hazards of radon mainly come from its progeny. In addition to natural radiation, the health effects caused by air pollution have gained significant attention from the scientific community and society [3]. Numerous epidemiological studies have demonstrated that exposure to elevated concentrations of ambient particulate matter (PM) pollution is a risk factor for cardiopulmonary diseases [4–6]. According to the World Health Organization (WHO), without reduction measures, air pollution will be the largest environmental issue responsible for premature death worldwide by 2050 [7]. Radon decay products easily combine with aerosol particles in the air, forming attached radon progenies [8], which can increase the short-term and/or long-term impacts on human health.

Air particulate matter monitoring commonly includes PM10 (mass of PM with an aerodynamic diameter less than or equal to 10 μm) and fine PM2.5 (mass of PM with an aerodynamic diameter less than or equal to 2.5 μm) [8]. Studies on the relationship between outdoor radon and its progeny concentrations and particulate matter concentrations have been reported both domestically and internationally. Chinese scholars have found that there were seasonal variations in atmospheric aerosol radioactivity and the relationship with total suspended particulate concentration was not simply linear [9,10]. Radon progeny concentration and PM2.5 showed a clear positive correlation [11], but there were some

differences, which may be related to meteorological factors, material sources, and measurement locations [12]. Moreover, there was a correlation between the concentration of attached radon progeny and both PM10 and PM2.5, but the correlation coefficient with PM2.5 was larger than that with PM10 [13]. Relevant studies by abroad scientists found that radon and PM10 have the highest concentration in winter and the lowest concentration in summer [14–17]. The correlation between radon concentration, PM2.5, and PM10 varied in different measurement environments, and the correlation coefficients also varied [18]. Meteorological parameters have significant impacts on radon concentration and air quality index. The concentration of radon and PM2.5 and ambient pressure showed reverse and direct correlation respectively. Increasing pressure and decreasing temperature caused all PM to increase, but the temperature was more sensitive [19]. However, Adeoye's research did not find a correlation between radon and PM2.5 or PM10 [20].

Extreme weather events, particularly haze and dust storms, can significantly increase particulate matter concentration in the air [21,22]. Due to the different formation mechanisms of haze and dust storms, there were differences in the composition of particulate pollutants in the air [23,24]. Previous studies have shown that the correlation between radon and its progeny concentrations, particulate matter concentrations, and meteorological parameters varies across different regions and seasons. However, few reports have investigated whether there are differences in the correlation between radon and its progeny concentrations and particulate matter concentrations under haze and dust storm weather. The frequent dust storms that occurred in Beijing during the spring of 2023 have caused significant adverse effects on human daily life. Therefore, this study analyzed the relationship between outdoor radon and its progeny concentrations, particulate matter concentrations, and meteorological parameters measured at the Radiation and Environment Laboratory of China University of Geosciences (Beijing) from March to April 2023. The results were compared with measurements taken during severe haze at the same location from November 2015 to January 2016. Furthermore, by incorporating canonical correlation analysis, we investigated the differences in the correlation between radon and its progeny concentrations, particulate matter concentrations, and meteorological parameters under haze and dust storm weather. In this study, we found that the impact of particulate matter concentration on radon and its progeny concentrations was higher during haze weather compared to dust storm weather. This can be primarily attributed to significantly higher PM2.5 concentrations during haze weather as compared to dust storm weather.

2. Materials and Methods

2.1. Data Collection

The instrument used for radon and its progeny measurement was the ERS-RDM-2S dual-channel radon/thoron and radon/thoron progeny monitor produced by Germany TRACERLAB GmbH, Köln, Germany. The detection efficiency of the device is 20%, and the lower limits of detection of radon and equivalent radon are approx. 15 and 0.1 Bq·m⁻³, respectively, at a 1 h counting interval [25]. The device was built with two silicon alpha-sensitive detectors (Canberra PIPS Sensitive Detector) and two alpha spectroscopy systems, MCA with 256 channels [25]. It is designed to collect the alpha particles of ²¹⁸Po and ²¹⁶Po for the determination of the concentration of radon and thoron, using the diffusion mode or pump mode. For the determination of the radon and thoron progeny concentration, ambient air is sucked by the internal air-suction pump with an airflow rate of approx. 100 L·h⁻¹ through the membrane filter (0.8 µm pore-size) of the removable progeny filter. There is a collection of ²¹⁸Po/²¹⁴Po for the determination of the radon progeny and ²¹²Po (a decay product of ²¹⁶Po) for the determination of the thoron progeny [25,26]. The instrument was calibrated in Physikalilisch-Technische Bundesanstalt, Braunschweig, Germany, the National Metrology Institute of Germany.

The measurement location selected for this study was a windowsill located south of the Radiation and Environment Laboratory of China University of Geosciences (Beijing) in Haidian District, Beijing, China. The windowsill is 2.16 m above the ground. The

actual measurement diagram is shown in Figure 1. During the measurement period, the instrument was placed indoors, while the radon/thoron detector and radon/thoron progeny detector were positioned outside the window to ensure sufficient contact with the outdoor atmosphere. Both detectors were placed in the same location, and the window was tightly closed without compressing the connection pipes of the detectors. The instrument operated in continuous measurement mode. The measurement time and mode were set as 1 h pump mode. The calculation of radon concentration and equilibrium equivalent radon concentration followed the methods described by Sun, 2017 and Wang, 2020 [11,26]. This study conducted measurements during two periods, with measurement periods from 22 March 2023, to 22 April 2023, and from 9 November 2015, to 9 January 2016, respectively. A total of 2091 sets of data were obtained, including 754 sets of radon concentration and equilibrium equivalent radon concentration data during 2023 and 1337 sets of data during 2015–2016.



Figure 1. Outdoor radon and its progeny concentration measurement.

Meteorological parameters and particulate matter concentrations were obtained from the data published by the website of the China Meteorological Administration (<http://www.weather.com.cn>) (9 November 2015–9 January 2016, and 22 March 2023–22 April 2023)) and the Air + Ecological Environment Big Data Service Platform (<https://www.dpt.daqi10.com/login.jsp>) (9 November 2015–9 January 2016, and 22 March 2023–22 April 2023)). During the measurement period, we recorded real-time parameter data from the nearest meteorological station at the Olympic Sports Center. These include atmospheric temperature, relative humidity, precipitation, wind force, wind direction, and PM_{2.5} and PM₁₀. Among them, wind force represents the intensity of the wind and is commonly expressed using wind scale in meteorology. There is a corresponding conversion relationship between the wind scale and the internationally used Beaufort scale. For specific details, please refer to “GB/T 28591-2012 Wind scale” [27].

2.2. Canonical Correlation Analysis

Canonical correlation analysis is a multivariate statistical analysis method that reflects the overall correlation between two sets of indicators by using comprehensive variables to represent their correlation. Its basic principle is to extract two representative comprehensive variables from each set of variables to grasp the overall correlation between the two sets of indicators. Then use the correlation between these two comprehensive variables to reflect the overall correlation between the two sets of indicators [28]. In this study, canonical

correlation analysis was performed using the canonical correlation function module in SPSS (Statistical Package for Social Science, Version 26).

In this study, radon and its progeny concentrations were treated as one set of variables, while particulate matter concentrations and meteorological parameters were treated as another set of variables. Normality tests were performed on both data sets. If both sets of data followed a normal distribution, canonical correlation analysis could be performed. The output of canonical correlation analysis includes canonical correlation, standardized canonical correlation coefficients, unstandardized canonical correlation coefficients, canonical loadings, cross-loadings, and the proportion of variance explained. By analyzing the results of canonical correlation and canonical loadings, the impact of each variable in particulate matter concentrations and meteorological parameters on radon and its progeny concentrations can be evaluated.

3. Results

3.1. Characteristics of Radon and Its Progeny Concentration

Normality tests were performed on the measured radon concentration (C_{Rn}) and equilibrium equivalent radon concentration (EEC-Rn) data, revealing that both C_{Rn} and EEC-Rn followed or approximately followed a normal distribution during the two consecutive measurement periods. The daily averages of C_{Rn} and EEC-Rn over time are shown in Figure 2. Both C_{Rn} and EEC-Rn exhibited large fluctuations with the change of measurement time during the two consecutive measurement periods. Combining the box plots of C_{Rn} and EEC-Rn (Figure 3), it can be seen that C_{Rn} was close with mean values of 19.77 ± 8.70 and 21.15 ± 9.72 $Bq \cdot m^{-3}$ during the two measurement periods from March to April 2023 (spring) and from November 2015 to January 2016 (winter), respectively, with ranges of 4–50 and 4–62 $Bq \cdot m^{-3}$, respectively. These values were significantly higher than the average radon levels in Beijing reported by Cheng et al. [29] and Peng et al. [30], which were 6.7 and 10.9 $Bq \cdot m^{-3}$, respectively. It cannot be ruled out that the differences in the results were influenced by the variations in measurement methods, such as measurement position, measurement height, etc. EEC-Rn exhibited distinct seasonal differences, with higher values in winter ranging from 1.78 to 19.92 $Bq \cdot m^{-3}$ and an average concentration of 9.06 ± 3.37 $Bq \cdot m^{-3}$. In contrast, the average concentration in spring was only 4.64 ± 2.53 $Bq \cdot m^{-3}$, with a range of 0.49–15.17 $Bq \cdot m^{-3}$. EEC-Rn in winter in this study was significantly higher than the reported average outdoor EEC-Rn in Beijing by Peng et al. (5.8 $Bq \cdot m^{-3}$) [30]. However, the results obtained in this study during the spring were similar to the findings of Peng et al. [30].

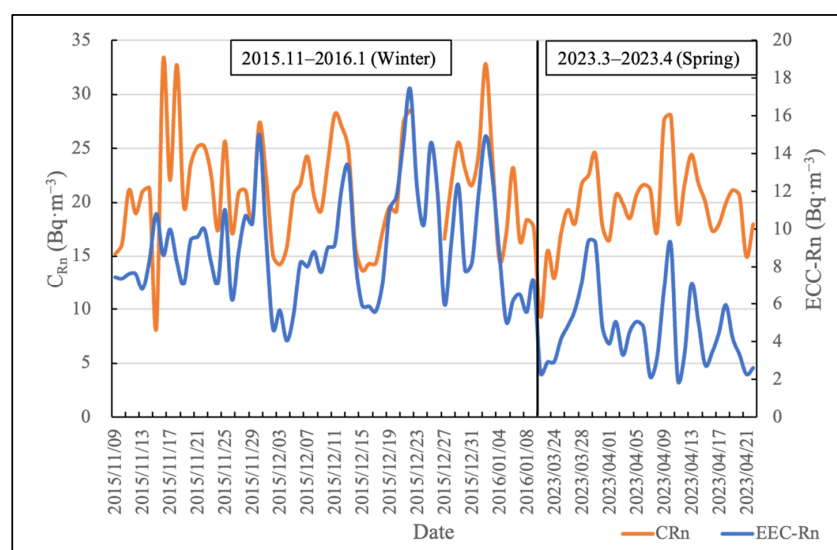


Figure 2. Daily variations in radon and equilibrium equivalent radon concentration.

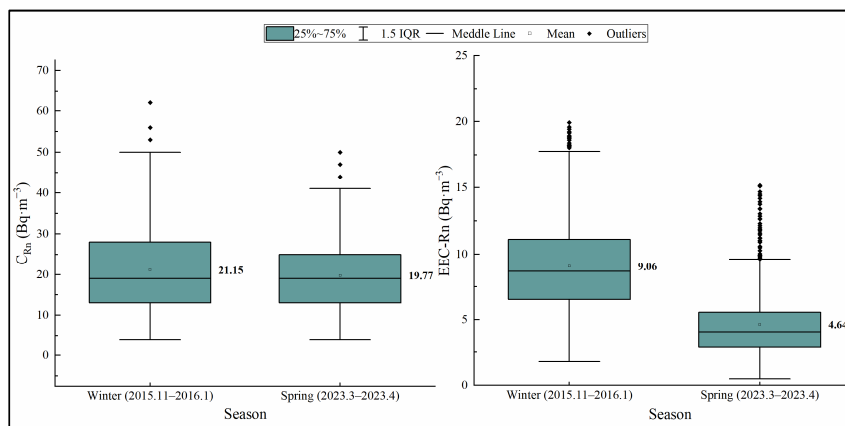


Figure 3. Seasonal variations in radon and equilibrium equivalent radon concentration.

To evaluate the diurnal variation, the average concentrations of C_{Rn} and EEC-Rn at the same time of day during the two consecutive measurement periods were calculated and sinusoidal functions were fitted to the data using Origin software, as shown in Figure 4. The diurnal variation pattern of C_{Rn} (Figure 4a) during the spring measurement period exhibited a clear “sine” characteristic ($R^2 = 0.76$), with the maximum value appearing around 5:00 and the minimum value appearing around 16:00. However, the diurnal variation pattern of C_{Rn} during the winter measurement period was not significant, with a low goodness of fit ($R^2 = 0.38$). The maximum and minimum values were observed around 6:00 and 18:00, respectively, slightly later than in the spring measurement period. Based on the fitted sinusoidal function of C_{Rn} , the amplitude of the fitted curve during the spring measurement period ($A = 2.54$) was about 2.3 times greater than that during the winter measurement period ($A = 1.11$). This indicates that the range and intensity of the diurnal variation in C_{Rn} were significantly higher in the spring compared to winter, which is consistent with the findings from the study conducted by Celikovic et al. [31].

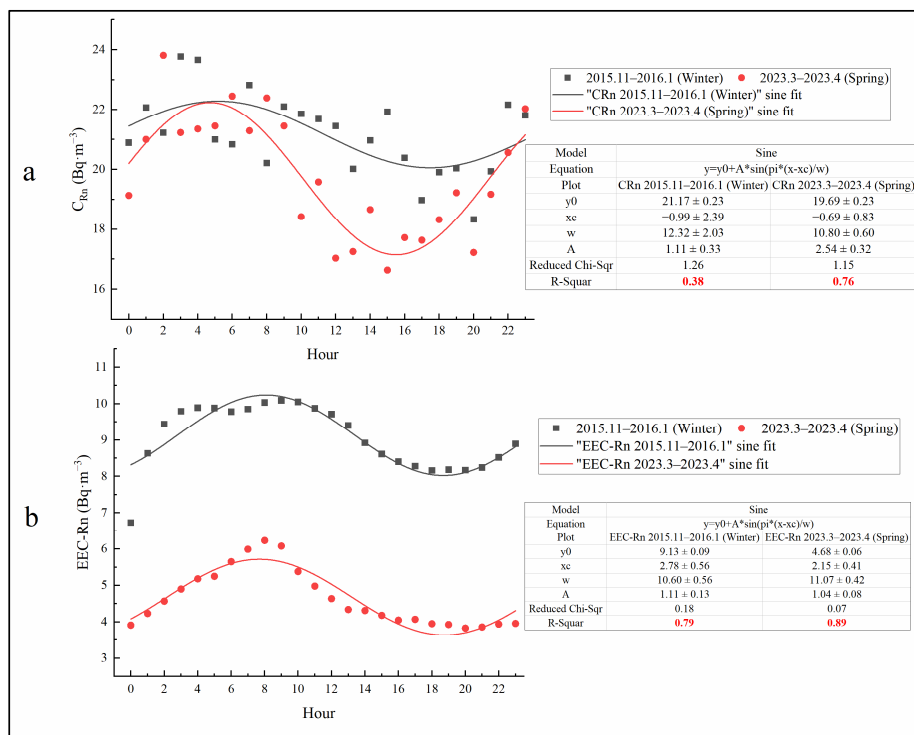


Figure 4. Diurnal variations in radon concentration (a) and equilibrium equivalent radon concentration (b).

The diurnal variation pattern of EEC-Rn (Figure 4b) exhibited a significant “sine” characteristic during both the spring and winter measurement periods, with goodness of fit values of 0.89 and 0.79, respectively. The maximum and minimum values of EEC-Rn appeared around 8:00 and 19:00, respectively, in both measurement periods. The range and intensity of the diurnal variation in EEC-Rn were similar in both measurement periods, with amplitudes (A) of 1.04 in spring and 1.11 in winter. Comparing the diurnal variation patterns of C_{Rn} and EEC-Rn, it can be seen that the maximum and minimum values of EEC-Rn appeared later than those of C_{Rn} in both measurement periods.

3.2. Characteristics of Particulate Matter Concentration and Meteorological Parameters

The air quality summary for the two consecutive measurement periods is presented in Table 1. During the measurement period from March to April 2023 (spring), approximately 41% of the total measurement days were classified as polluted days. Out of the total measurement days, 18 days were recorded as dust storm days, accounting for 56% of the total measurement days. In the measurement period from November 2015 to January 2016 (winter), nearly 60% of the total measurement days were polluted days, with 30 recorded haze days accounting for approximately 48% of the total measurement days.

Table 1. Air quality summary (days) during the two measurement periods.

Air Quality	November 2015 to January 2016 (Winter)	March to April 2023 (Spring)
Excellent	15	6
Good	10	13
Pollution ¹	37	13
Proportion of polluted days	59.68%	40.63%

¹ Pollution includes mild pollution, moderate pollution, heavy pollution, and severe pollution.

The variation in PM_{2.5} and PM₁₀ concentrations over time is shown in Figure 5. During both consecutive measurement periods, there was a significant positive correlation between PM_{2.5} and PM₁₀ concentrations, with correlation coefficients greater than 0.9. The average concentration of PM_{2.5} during the spring measurement period was significantly lower than that during the winter measurement period, with mean values of 53.65 and 139.84 $\mu\text{g}\cdot\text{m}^{-3}$, respectively. The range in variations during both periods was up to two orders of magnitude, ranging from 4.88–186.50 and 5.94–507.30 $\mu\text{g}\cdot\text{m}^{-3}$, respectively. The average concentration of PM₁₀ during the spring and winter consecutive measurement periods was close, with values of 148.20 and 182.83 $\mu\text{g}\cdot\text{m}^{-3}$, respectively. The range in variation was 30.75–584.04 and 5.00–590.54 $\mu\text{g}\cdot\text{m}^{-3}$, respectively. Comparing the proportion of PM_{2.5} to PM₁₀ between the two measurement periods, it was found that the ratio of PM_{2.5} to PM₁₀ during the winter measurement period was significantly higher than that during the spring measurement period, with values of 76.5% and 36.2%, respectively.

We have also collected data on the maximum PM_{2.5} concentrations and their percentages in PM₁₀ recorded during dust storms in various countries/regions [32–36], as presented in Table 2. During dust storms, the PM_{2.5} concentrations recorded in this study were significantly higher than those reported in Rome, America, and Belgium, but significantly lower than those recorded in Mongolia and Korea. As for the ratio of PM_{2.5} to PM₁₀, the results of this study were similar to those obtained in Rome, Mongolia, and Belgium, and significantly higher than those in Korea and America.

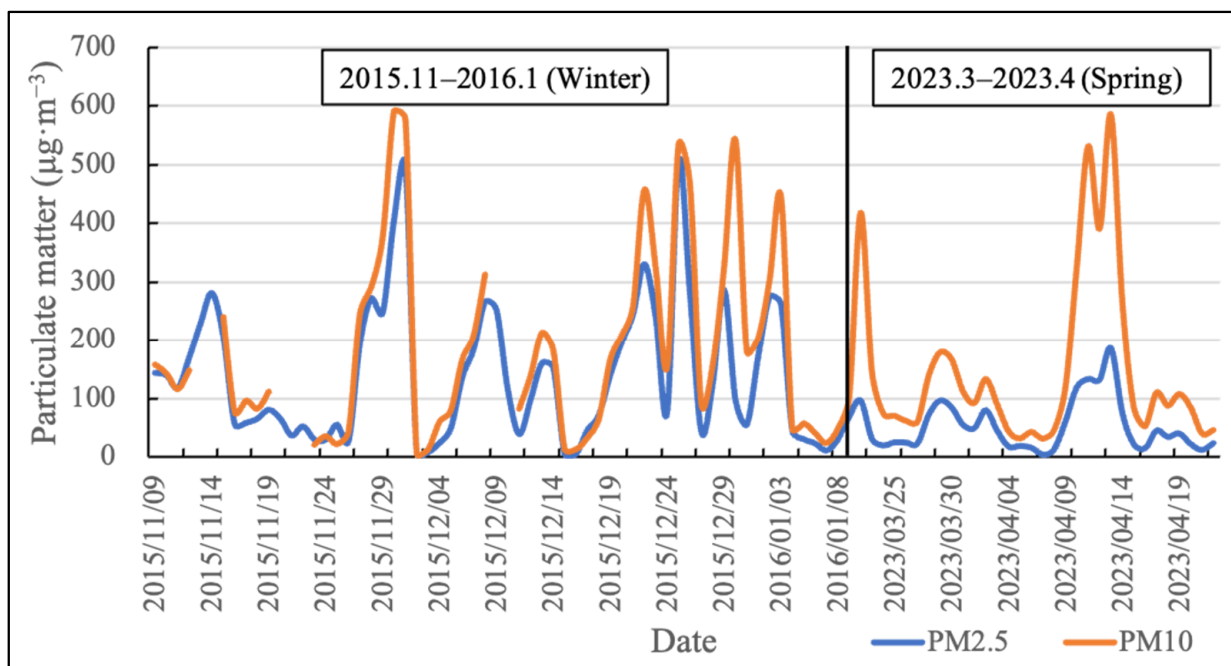


Figure 5. Daily variations in PM2.5 and PM10 concentration.

Table 2. Maximum PM2.5 concentrations ($\mu\text{g}\cdot\text{m}^{-3}$) and their percentage of PM10 in dust storms observed in different countries/regions.

Location	PM2.5	% of PM10	Reference
Beijing	186.5	36.2	Present study
Rome	86.0	47.3	[32]
Mongolia	700.0	36.3	[33]
Korea	294.0	10.0	[34]
America	55.7	13.1	[35]
Belgium	43.0	42.8	[36]

The daily mean values of atmospheric temperature (T), relative humidity (RH), and wind force (W) recorded during the two consecutive measurement periods are shown in Figure 6a. There were significant differences in T and RH between the spring and winter consecutive measurement periods. The average values of T and RH during the spring were 13.79 °C and 40.07%, respectively, while during the winter, they were 0.24 °C and 65.91%, respectively. The recorded values of W were similar during both the spring and winter measurement periods, with average values of 1.65 and 1.58, respectively. Comparing the diurnal variations in T, RH, and W (Figure 6b), it can be seen that the variations in T and RH in the spring exhibited a “sine” characteristic, while in the winter, they showed a near “single-peak” shape. The range in T and RH variation in the spring was significantly larger than that in the winter. The variation pattern of W was consistent in both the spring and winter, showing a “sine” shape, but with a larger range in variation in the spring than in the winter. The diurnal extreme values of T, RH, and W appeared around 6:00 and 15:00, respectively. Among them, the minimum values of T and W occurred around 6:00, while the maximum values occurred around 15:00. RH exhibited the opposite trend, with around 6:00 showing the maximum value and around 15:00 showing the minimum value.

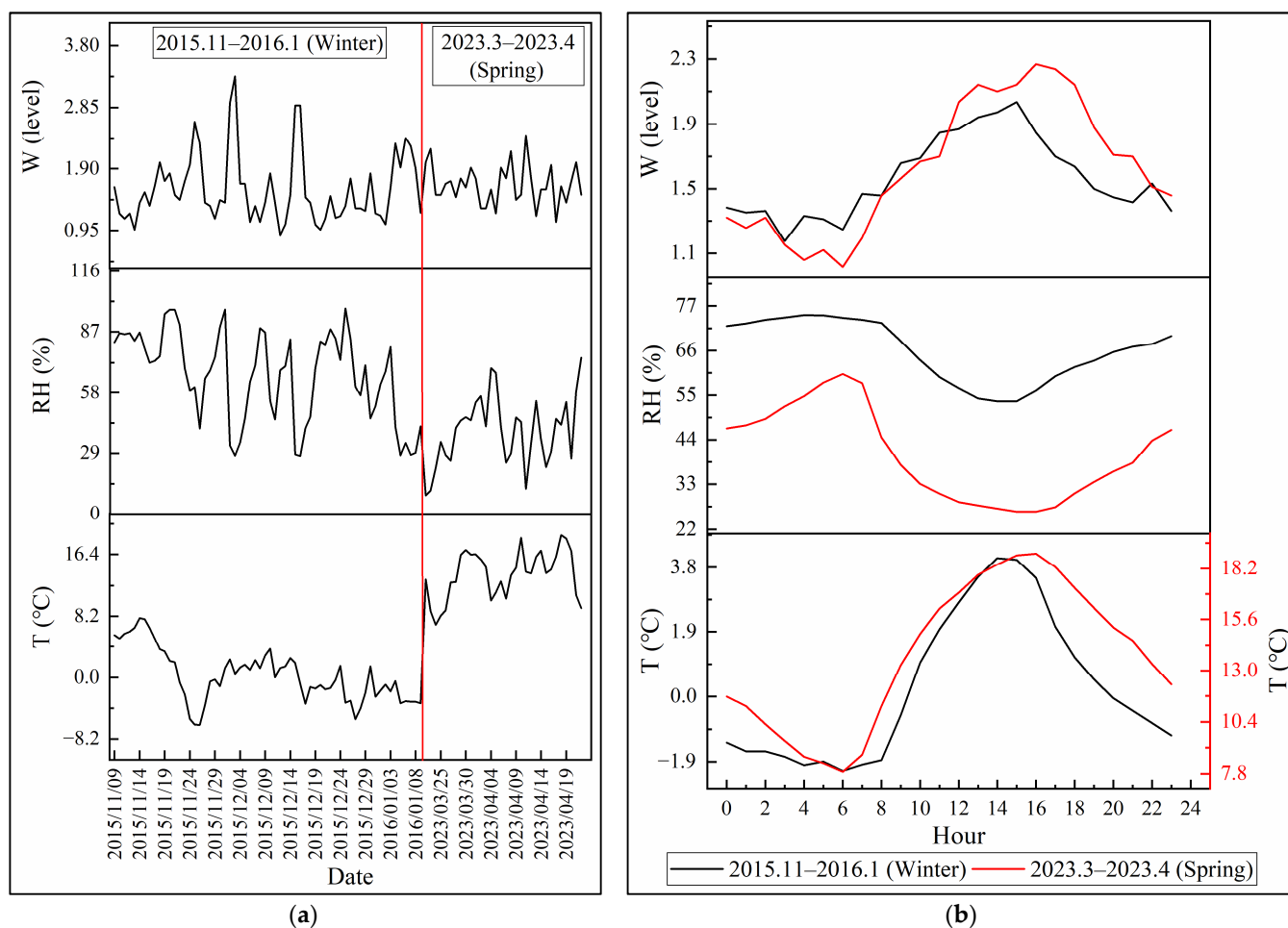


Figure 6. Daily variations (a) and diurnal variations (b) in atmospheric temperature (T), relative humidity (RH), and wind force (W).

3.3. Relationships between Radon and Its Progeny Concentrations and Particulate Matter Concentrations and Meteorological Parameters

Pearson correlation analysis was performed to determine the correlations between C_{Rn} , EEC-Rn, PM concentrations, and meteorological parameters, and the results are shown in Figure 7. Due to variations in meteorological parameters recorded during two distinct measurement periods, certain parameters, such as precipitation (P) during the period from November 2015 to January 2016, and atmospheric pressure (AP) during the period from March 2023 to April 2023, were not recorded. Consequently, there are differences in the Pearson correlation analysis between these two distinct measurement periods for individual parameters. During the two consecutive measurement periods, both C_{Rn} and EEC-Rn exhibited positive correlations with relative humidity (RH), PM_{2.5}, and PM₁₀. However, the correlation coefficients were significantly higher in the winter than in the spring. To explore the influence of wind direction, the directions were digitized and shown in Figure 8. The numbers increased sequentially in the clockwise direction. Both C_{Rn} and EEC-Rn showed strong negative correlations with wind force (W) and wind direction (WD) during the two measurement periods. C_{Rn} and EEC-Rn were positively correlated with temperature (T) in the spring, but showed no correlation in the winter. Furthermore, C_{Rn} and EEC-Rn were positively correlated with precipitation (P) in the spring, while being negatively correlated with atmospheric pressure (AP) in the winter. Strong correlations were also observed between PM concentrations and meteorological parameters.

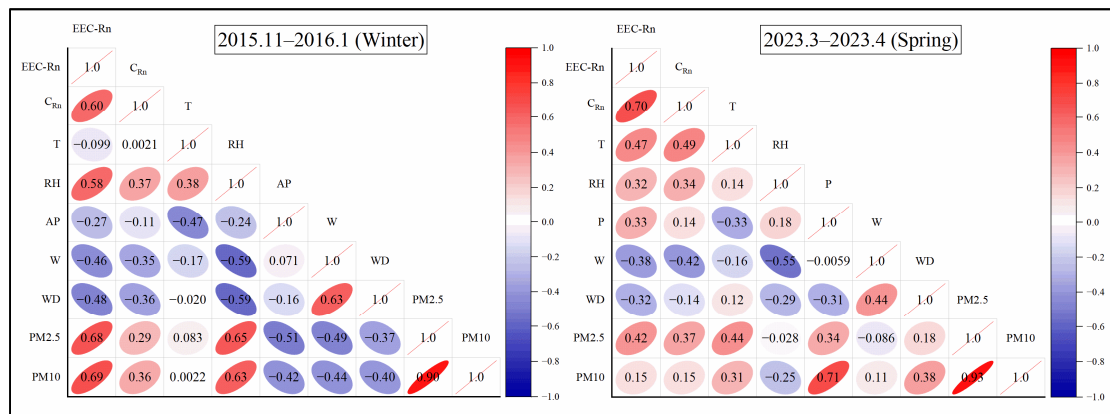


Figure 7. Correlation between radon and its progeny concentrations and particulate matter concentrations and meteorological parameters. T—atmospheric temperature; AP—atmospheric pressure; RH—relative humidity; P—precipitation; W—wind force; WD—wind direction, the same below.

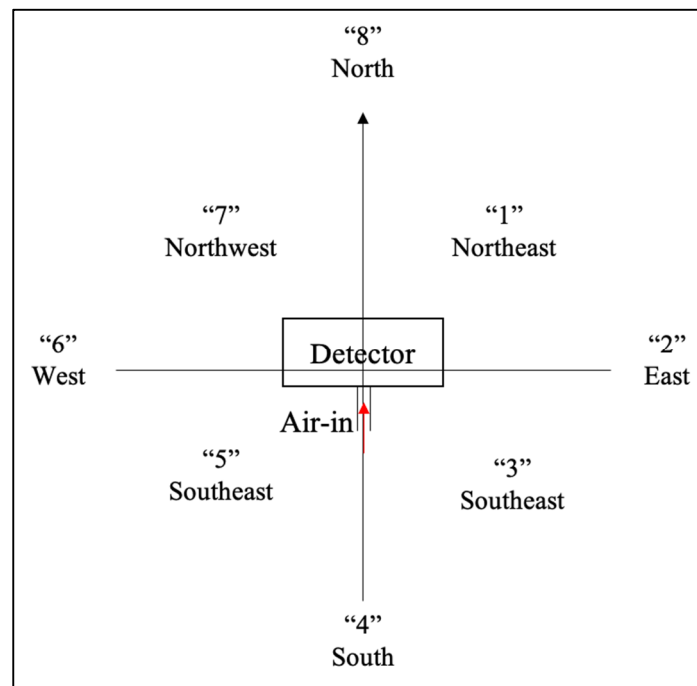


Figure 8. Digitization of directions and orientation of the detector. The direction of the red arrow in the figure is the direction of air-in.

The Pearson correlation analysis results revealed that there were correlations between radon and its progeny concentrations, PM concentrations, and meteorological parameters. Moreover, significant correlations were observed between PM concentrations and meteorological parameters. This indicates that changes in radon and its progeny concentrations are influenced by a combination of PM concentrations and meteorological parameters. It is important to note that analyzing correlations between two parameters alone may not provide a comprehensive understanding of the situation. To further explore the relationships between the variables, the parameters were divided into two groups: group A variables included C_{Rn} and EEC-Rn, while group B variables included PM2.5, PM10, T, AP, RH, W, and WD. It is crucial to emphasize that, to maintain comparability in the results of the canonical correlation analysis between the two measurement periods, we specifically chose meteorological parameters that were recorded during both measurement periods as independent variables. What is more, during haze or dust storm weather, atmospheric

precipitation is generally absent. Therefore, the variable P was not included in the canonical correlation analysis. Canonical correlation analysis was conducted using SPSS software to analyze the relationships between the A and B variables.

The results of the canonical correlation analysis are presented in Table 3. During the two consecutive measurement periods, the correlation coefficients for the first canonical variable were 0.80 and 0.81, respectively, with both being significant at the 0.01 level. The significance of the second canonical variable was greater than 0.05, indicating that variables A and B were significantly positively correlated only with the first canonical variable.

Table 3. Canonical correlation analysis results.

Canonical Variation	Correlation	Eigenvalue	Wilks Statistic	Sig.
1	0.80	1.75	0.33	0.00
2	0.29	0.09	0.92	0.68
March to April 2023 (Spring)				
1	0.81	1.85	0.32	0.00
2	0.31	0.11	0.90	0.74

H0 for Wilks test is that the correlations in the current and following rows are zero.

The canonical loading coefficients of variables A and B in the first canonical variable during the two consecutive measurement periods are shown in Figure 9. During the winter measurement period when haze frequently occurs (Figure 9a), the loading coefficients of PM concentrations in variable B were significantly higher than those of meteorological parameters. Specifically, the changes in T had almost no effect on variable B, as its loading coefficient was close to 0. Combined with the significant positive influence between variables A and B, it can be concluded that PM2.5, PM10, and RH had significant positive effects on EEC-Rn and C_{Rn}, while W and WD had negative effects on EEC-Rn and C_{Rn}. The degree of influence from high to low was PM2.5, PM10, RH, WD, and W. The impact of each parameter on EEC-Rn was approximately twice as much as its impact on C_{Rn}.

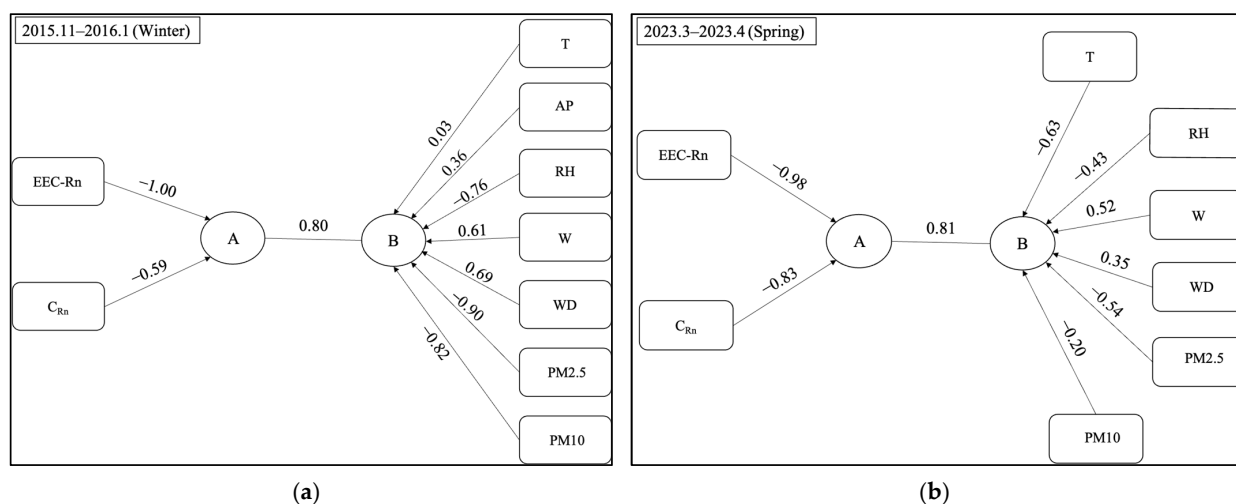


Figure 9. Canonical loading coefficients of each variable, (a) November 2015–January 2016 (winter); (b) March 2023–April 2023 (spring). C_{Rn}—radon concentration; EEC-Rn—equilibrium equivalent radon concentration; A & B—group variables; T—atmospheric temperature; AP—atmospheric pressure; RH—relative humidity; W—wind force; WD—wind direction.

During the spring measurement period when dust storms frequently occur (Figure 9b), the weights of the influence of EEC-Rn and C_{Rn} in variable A were similar, with loading coefficients of −0.98 and −0.83, respectively. In variable B, the influences of each parameter

were similar, except for the significantly lower influence of PM₁₀. Based on the significant positive influence between variables A and B, it can be concluded that T, PM_{2.5}, and RH had positive effects on EEC-Rn and C_{Rn}, while W and WD had negative effects on EEC-Rn and C_{Rn}. The degree of influence of each parameter on EEC-Rn and C_{Rn} was from high to low in the following order: T, PM_{2.5}, W, RH, WD, and PM₁₀.

4. Discussion

The diurnal variation pattern of C_{Rn} and EEC-Rn shows a maximum in the early morning and a minimum in the late afternoon, which is related to the vertical distribution of T at the ground level [37–39]. Combining the diurnal variation in T shown in Figure 6b, it can be observed that the diurnal range and intensity of T in spring are significantly greater than in winter. The diurnal variation pattern of T in winter is close to a “single peak” shape, with T remaining relatively stable from 0:00 to 8:00 and gradually increasing thereafter. This pattern is opposite to the diurnal variation pattern of C_{Rn} in winter, where C_{Rn} starts to decrease from 8:00. T influences the mixing depth of the atmosphere [39]. During the nighttime, a temperature inversion is formed between the ground and the atmosphere, resulting in a decrease in the mixing depth of the atmosphere. At this time, the diffusion of radon near the ground surface is limited, leading to the accumulation of C_{Rn}. As the sun rises in the morning, the temperature inversion between the ground and the atmosphere is disrupted. During the day, a large vertical temperature difference occurs, increasing the mixing depth of the atmosphere and allowing radon near the ground surface to diffuse more easily. The vertical temperature difference reaches its maximum in the late afternoon, resulting in the lowest C_{Rn} at that time. The time difference in the occurrence of maximum and minimum values in the diurnal variation pattern of C_{Rn} between spring and winter is significantly related to the time when the T reaches its extreme values. The differences in the range and intensity of diurnal C_{Rn} variation in winter and spring are related to the intensity and duration of solar radiation. In comparison to spring, winter has longer nighttime duration, leading to shorter sunlight exposure during the day. This results in a greater diurnal variation intensity of C_{Rn} in spring than in winter.

When comparing the measurement results during dust storms period with other countries/regions listed in Table 2, we found that, apart from Mongolia, the PM_{2.5} levels obtained in this study and their percentage in PM₁₀ were close to those of most countries/regions. In Mongolia, the maximum measured value of PM_{2.5} was 700 µg·m⁻³, attributed to the measurement site located in the Gobi Desert. Mongolia is an arid–semi-arid region, with most areas located in the Gobi and desert zones, which leads to significantly higher particulate matter concentrations due to proximity to local sources [33,40]. Although the PM_{2.5} concentrations obtained in this study were significantly lower than those in Mongolia, the percentage of PM_{2.5} in PM₁₀ was similar. By comprehensively comparing the results of this study with those from other countries/regions, it can be concluded that the notable difference in particulate matter concentration characteristics between dust storm weather and haze weather is that the percentage of PM_{2.5} in PM₁₀ is significantly lower during dust storms compared to haze episodes.

Combining the results of both Pearson correlation analysis and canonical correlation analysis of various parameters, it is clear that PM concentration is the primary influencing factor of EEC-Rn in winter, followed by RH. This is attributed to the frequent occurrence of haze weather during the winter measurement period, resulting in relatively high concentrations of PM_{2.5} and PM₁₀, which promote the increase of EEC-Rn. Additionally, relatively high RH can enhance the attachment of radon progeny to aerosols [12]. The influence of PM_{2.5} and PM₁₀ on EEC-Rn is significantly greater than that on C_{Rn} due to the radon not readily adhering to aerosols. In spring, both PM_{2.5} and PM₁₀ exhibit positive correlations with C_{Rn} and EEC-Rn, but the impact is significantly reduced compared to winter. This is because the pollution during the spring measurement period is mainly from dust storms. Due to different sources and formation processes of pollutants, the composition of atmospheric pollutants differs between haze weather and dust storm weather [23,24].

Consequently, the effect of PM_{2.5} and PM₁₀ concentration on C_{Rn} and EEC-Rn differ significantly between the winter and spring measurement periods. This is further supported by the significant difference in PM_{2.5} concentrations recorded between the two measurement periods. In addition, the recorded PM₁₀ concentrations were close between spring and winter, but their correlations with C_{Rn} and EEC-Rn displayed significant differences. This is because PM₁₀ concentrations with an aerodynamic diameter of less than 10 μm include the concentrations of PM_{2.5}. When PM₁₀ concentrations are close, the considerably lower PM_{2.5} concentrations lead to a substantial reduction in the correlation between PM₁₀ and C_{Rn} and EEC-Rn. Therefore, the correlations between PM concentration and C_{Rn} and EEC-Rn are mainly manifested in the correlation between PM_{2.5} and C_{Rn} and EEC-Rn.

There are differences in the influence of meteorological parameters and PM concentrations on C_{Rn} and EEC-Rn between haze and dust storm weather conditions. In dust storm weather, where fine particles (PM_{2.5}) concentrations are considerably lower than PM₁₀ concentrations, the influence of meteorological parameters becomes more dominant. In contrast, in haze weather characterized by significantly higher PM_{2.5} concentrations, the impact of PM concentrations surpasses that of meteorological parameters. Therefore, it can be concluded that when PM concentrations are significantly elevated, PM concentrations serve as the primary influencing factor for C_{Rn} and EEC-Rn. However, when PM concentrations are relatively low, the impact of meteorological parameters on C_{Rn} and EEC-Rn becomes more pronounced.

5. Conclusions

This study measured the concentrations of radon and its progeny in outdoor air during the frequent haze period from November 2015 to January 2016 and the frequent dust storm period from March 2023 to April 2023. Simultaneously, particulate matter concentrations and various meteorological parameters were recorded. We analyzed the correlations between radon and its progeny concentrations, particulate matter concentrations, and meteorological parameters during these two measurement periods. Furthermore, by incorporating canonical correlation analysis, the differences in the correlation between radon and its progeny concentrations and particulate matter concentrations during the two pollution weather periods were investigated. The following conclusions were drawn:

1. Outdoor radon and its progeny concentrations display a diurnal variation pattern with a maximum in the early morning and a minimum in the late afternoon. The diurnal variation intensity of radon concentration is significantly influenced by the intensity of atmospheric temperature. Radon concentrations do not show significant seasonal variations, but equilibrium equivalent radon concentrations are significantly lower in spring than in winter. During dust storm weather, the concentration of PM_{2.5} and the percentage of PM_{2.5} in PM₁₀ in the air are notably lower compared to haze weather.
2. Radon and its progeny concentrations are positively correlated with particulate matter concentrations, but the correlation is significantly stronger during haze weather than during dust storm weather. The disparity in the correlation between radon and its progeny and particulate matter concentration during different types of polluted weather is influenced by the concentration of PM_{2.5}. Notably, a higher percentage of PM_{2.5} in PM₁₀ was observed during haze weather than during dust storm weather.
3. Particulate matter, mainly PM_{2.5}, has a significant effect on the concentration of radon and its progeny. When particulate matter concentrations are elevated, the influence of meteorological parameters on radon and its progeny concentrations is less significant compared to the influence of particulate matter concentrations. Wind level and wind direction have significant negative impacts on radon and its progeny concentrations, particularly during the winter when haze events are frequent.

Based on the conclusions drawn, it is recommended to strengthen the monitoring of radon and its progeny concentrations, as well as particulate matter concentrations, during pollution weather conditions. This would provide valuable data for assessing the extent

of exposure and identifying areas of high risk, enabling effective mitigation strategies to be implemented.

Supplementary Materials: The following supporting information can be downloaded at: <https://www.mdpi.com/article/10.3390/atmos14071132/s1>.

Author Contributions: Conceptualization, C.Y. and N.W.; methodology, C.Y.; software, C.Y.; validation, C.Y., Y.S. and N.W.; formal analysis, C.Y.; investigation, C.Y. and Y.S.; resources, N.W.; data curation, C.Y. and Y.S.; writing—original draft preparation, C.Y.; writing—review and editing, C.Y. and N.W.; visualization, C.Y.; supervision, N.W.; project administration, N.W.; funding acquisition, N.W. All authors have read and agreed to the published version of the manuscript.

Funding: This research was funded by the National Natural Science Foundation of China, grant numbers 41974167 and 41674111.

Institutional Review Board Statement: The study did not require ethical approval.

Informed Consent Statement: Not applicable.

Data Availability Statement: The data presented in this study were uploaded as a Supplementary File.

Acknowledgments: The authors would like to thank Mengke Han and Ying Jiang, at the Radiation Environment Laboratory of China University of Geosciences (Beijing), for their valuable advice during the preparation of this manuscript.

Conflicts of Interest: The authors declare no conflict of interest.

References

1. ICRP. *Lung Cancer Risk from Radon and Progeny and Statement on Radon*; ICRP Publication 115, Ann. ICRP 40(1); Elsevier: Amsterdam, The Netherlands, 2010.
2. UNSCEAR. *Sources and Effects of Ionizing Radiation, United Nations Scientific Committee on the Effects of Atomic Radiation*; UNSCEAR 2000 Report to the General Assembly, with Scientific Annexes, Volume I: Sources; United Nations: New York, NY, USA, 2000.
3. EEA. *Air Quality in Europe 2022*; European Environment Agency Report No. 05/2022; European Environment Agency: Copenhagen K, Denmark, 2022; Available online: <https://www.eea.europa.eu/publications/air-quality-in-europe-2022> (accessed on 3 June 2023).
4. Katsouyanni, K.; Touloumi, G.; Samoli, A.; Gryparis, A.; Le Tertre, A.; Monopoli, Y.; Rossi, G.; Zmirou, D.; Ballester, F.; Boumghar, A.; et al. Confounding and Effect Modification in the Short-Term Effects of Ambient Particles on Total Mortality: Results from 29 European Cities within the APHEA2 Project. *Epidemiology* **2001**, *12*, 521–531. Available online: <http://www.jstor.org/stable/3703877> (accessed on 1 June 2023). [\[CrossRef\]](#)
5. Tian, F.; Qi, J.; Wang, L.; Yin, P.; Qian, Z.; Ruan, Z.; Liu, J.; Liu, Y.; McMillin, S.E.; Wang, C.; et al. Differentiating the effects of ambient fine and coarse particles on mortality from cardiopulmonary diseases: A nationwide multicity study. *Environ. Int.* **2020**, *145*, 106096. [\[CrossRef\]](#)
6. Chen, R.; Yin, P.; Meng, X.; Wang, L.; Liu, C.; Niu, Y.; Liu, Y.; Liu, J.; Qi, J.; You, J.; et al. Associations between coarse particulate matter air pollution and cause-specific mortality: A nationwide analysis in 272 Chinese cities. *Environ. Heal. Perspect.* **2019**, *127*, 017008. [\[CrossRef\]](#)
7. WHO; Regional Office for Europe. *Evolution of WHO Air Quality Guidelines: Past, Present and Future*; World Health Organization, Regional Office for Europe: Geneva, Switzerland, 2017; Available online: <https://apps.who.int/iris/handle/10665/341912> (accessed on 2 June 2023).
8. Tokonami, S. Experimental verification of the attachment theory of radon progeny onto ambient aerosols. *Health Phys.* **2000**, *78*, 74–79. [\[CrossRef\]](#)
9. Gao, X. A Preliminary Study on the Radioactive Activity of Atmospheric Aerosols. *Shaanxi Environ.* **1997**, *4*, 21–24. (In Chinese)
10. Xi, H.; Wei, S.; Sha, C. Discussion on the Influence of Aerosols and the Change of Radon Concentration to Radon Daughter. *Technol. Sq.* **2014**, *3*, 18–21. (In Chinese) [\[CrossRef\]](#)
11. Sun, Y. A Study of Correlation between Concentrations of Outdoor Radon Including Its Progenies and PM2.5 in Beijing Area. Master's Thesis, China University of Geosciences, Beijing, China, 2017.
12. Wang, M.; Pan, Z.; Liu, S.; Chen, L.; Liao, J. Validation of the Correlation between Outdoor Concentrations of PM2.5 and short-lived Radon Progenies. *Chin. J. Radiol. Health* **2017**, *26*, 133–136. (In Chinese) [\[CrossRef\]](#)
13. Song, L. Studies on Distribution Characteristics of Radionuclides in the Fog Haze Weather. Master's Thesis, Soochow University, Jiangsu, China, 2015.
14. Zoran, M.; Savastru, D.; Dida, A. Assessing urban air quality and its relation with radon (^{222}Rn). *J. Radioanal. Nucl. Chem.* **2016**, *309*, 909–922. [\[CrossRef\]](#)

15. Zoran, M.A.; Savastru, R.S.; Savastru, D.M.; Penache, M.-C.V. Temporal trends of carbon monoxide (CO) and radon (^{222}Rn) tracers of urban air pollution. *J. Radioanal. Nucl. Chem.* **2019**, *320*, 55–70. [[CrossRef](#)]
16. Zoran, M.A.; Dida, M.R.; Zoran, A.; Zoran, L.F.; Dida, A. Outdoor ^{222}Rn concentrations monitoring in relation with particulate matter levels and possible health effects. *J. Radioanal. Nucl. Chem.* **2013**, *296*, 1179–1192. [[CrossRef](#)]
17. Zoran, M.; Dida, M.R.; Savastru, R.; Savastru, D.; Dida, A.; Ionescu, O. Ground level ozone (O_3) associated with radon (^{222}Rn) and particulate matter (PM) concentrations in Bucharest metropolitan area and adverse health effects. *J. Radioanal. Nucl. Chem.* **2014**, *300*, 729–746. [[CrossRef](#)]
18. Kubiak, J.A.; Basińska, M. Analysis of the Radon Concentration in Selected Rooms of Buildings in Poznan County. *Atmosphere* **2022**, *13*, 1664. [[CrossRef](#)]
19. Kazemi, K.V.; Mansouri, N.; Moattar, F.; Khezri, S.M. Characterization of indoor/outdoor PM₁₀, PM_{2.5}, PM₁ and radon concentrations in Imam Khomeini hospital. *Bulg. Chem. Commun.* **2016**, *48*, 345–350.
20. Adeoye, C.; Gupta, J.; Demers, N.; Adhikari, A. Variations of radon and airborne particulate matter near three large phosphogypsum stacks in Florida. *Environ. Monit. Assess.* **2021**, *193*, 284. [[CrossRef](#)]
21. Elahi, E.; Khalid, Z.; Tauni, M.Z.; Zhang, H.; Lirong, X. Extreme weather events risk to crop-production and the adaptation of innovative management strategies to mitigate the risk: A retrospective survey of rural Punjab, Pakistan. *Technovation* **2022**, *117*, 102255. [[CrossRef](#)]
22. Abbas, A.; Waseem, M.; Ullah, W.; Zhao, C.; Zhu, J. Spatiotemporal Analysis of Meteorological and Hydrological Droughts and Their Propagations. *Water* **2021**, *13*, 2237. [[CrossRef](#)]
23. Zaady, E.; Offer, Z.Y.; Shachak, M. The content and contribution of deposited aeolian organic matter in a dry land ecosystem of the Negev Desert, Israel. *Atmos. Environ.* **2001**, *35*, 769–776. [[CrossRef](#)]
24. Goudie, A.S. Desert dust and human health disorders. *Environ. Int.* **2014**, *63*, 101–113. [[CrossRef](#)]
25. Tracerlab. *ERS-RDM-2S Monitor for the Determination of the Radon/Thoron-Gas- & Progeny Concentration, Short-Version-2017/08*; Tracerlab GmbH: Koeln, Germany, 2017.
26. Wang, N.; Hu, M.; Zeng, W.; Yu, C.; Jia, B.; Yang, Z. Indoor and outdoor ^{222}Rn and ^{220}Rn and their progeny levels surrounding Bayan Obo mine, China. *Nukleonika* **2020**, *65*, 145–148. [[CrossRef](#)]
27. GB/T 28591-2012; Wind Scale. General Administration of Quality Supervision, Inspection and Quarantine of the People's Republic of China & Standardization Administration of the People's Republic of China, Standards Press of China: Beijing, China, 2012. (In Chinese)
28. Hardoon, D.R.; Szedmak, S.; Shawe-Taylor, J. Canonical Correlation Analysis: An Overview with Application to Learning Methods. *Neural Comput.* **2004**, *16*, 2639–2664. [[CrossRef](#)] [[PubMed](#)]
29. Cheng, J.; Guo, Q.; Ren, T. Radon Levels in China. *J. Nucl. Sci. Technol.* **2002**, *39*, 695–699. [[CrossRef](#)]
30. Gao, P.; Wang, Y.; Song, Z.Y.; Sun, X. Study on outdoor radon and its progeny concentration level and variation pattern in Beijing area. *Chin. J. Radiol. Health* **2020**, *40*, 698–701. [[CrossRef](#)]
31. Čeliković, I.; Pantelić, G.; Vukanac, I.; Nikolić, J.K.; Živanović, M.; Cinelli, G.; Gruber, V.; Baumann, S.; Poncela, L.S.Q.; Rabago, D. Outdoor Radon as a Tool to Estimate Radon Priority Areas—A Literature Overview. *Int. J. Environ. Res. Public Health* **2022**, *19*, 662. [[CrossRef](#)] [[PubMed](#)]
32. Mallone, S.; Stafoggia, M.; Faustini, A.; Gobbi, G.P.; Marconi, A.; Forastiere, F. Saharan Dust and Associations between Particulate Matter and Daily Mortality in Rome, Italy. *Environ. Heal. Perspect.* **2011**, *119*, 1409–1414. [[CrossRef](#)] [[PubMed](#)]
33. Dement'eva, A.L.; Zhamsueva, G.S.; Zayakhanov, A.S.; Tsydygov, V.V.; Ayurzhanov, A.A.; Azzayaa, D.; Oyunchimeg, D. Mass concentration of PM₁₀ and PM_{2.5} fine-dispersed aerosol fractions in the Eastern Gobi Desert. *Russ. Meteorol. Hydrol.* **2013**, *38*, 80–87. [[CrossRef](#)]
34. Chung, Y.; Kim, H.; Dulam, J.; Harris, J. On heavy dustfall observed with explosive sandstorms in Chongwon-Chongju, Korea in 2002. *Atmos. Environ.* **2003**, *37*, 3425–3433. [[CrossRef](#)]
35. Hahnenberger, M.; Nicoll, K. Meteorological characteristics of dust storm events in the eastern Great Basin of Utah, U.S.A. *Atmos. Environ.* **2012**, *60*, 601–612. [[CrossRef](#)]
36. Vanderstraeten, P.; Lénelle, Y.; Meurrens, A.; Carati, D.; Brenig, L.; Delcloo, A.; Offer, Z.; Zaady, E. Dust storm originate from Sahara covering Western Europe: A case study. *Atmos. Environ.* **2008**, *42*, 5489–5493. [[CrossRef](#)]
37. Zhuo, W.; Furukawa, M.; Guo, Q.; Kim, Y.S. Soil radon flux and outdoor radon concentrations in East Asia. *Int. Congr. Ser.* **2005**, *1276*, 285–286. [[CrossRef](#)]
38. Zhang, L.G.; Guo, Q.J.; Lida, T. Atmospheric radon levels in Beijing, China. *Radiat. Prot. Dosim.* **2004**, *112*, 449–453. [[CrossRef](#)]
39. Kikaj, D.; Chambers, S.D.; Crawford, J.; Kobal, M.; Gregorič, A.; Vaupotič, J. Investigating the vertical and spatial extent of radon-based classification of the atmospheric mixing state and impacts on seasonal urban air quality. *Sci. Total Environ.* **2023**, *872*, 162126. [[CrossRef](#)] [[PubMed](#)]
40. Natsagdorj, L.; Jugder, D.; Chung, Y.S. Analysis of dusts storms observed in Mongolia during 1937–1999. *Atmos. Environ.* **2003**, *37*, 1401–1411. [[CrossRef](#)]

Disclaimer/Publisher's Note: The statements, opinions and data contained in all publications are solely those of the individual author(s) and contributor(s) and not of MDPI and/or the editor(s). MDPI and/or the editor(s) disclaim responsibility for any injury to people or property resulting from any ideas, methods, instructions or products referred to in the content.